PAPER

Check for updates

Gold nanoparticle SERS substrates sustainable at extremely high temperatures

Fernando D. Cortes Vega,[ab] Pablo G. Martinez Torres,*[c] Juan Pichardo Molina,[d] Nikte M. Gomez Ortiz,[d] Viktor G. Hadjiev,[e] Juan Zarate Medina[a] and Francisco C. Robles Hernandez [ID] *[bf]

We report a technology for supporting gold nanoparticles (GNPS) with preserved SERS activity in substrates capable of sustaining temperatures as high as the melting point of gold. The material processing involved dispersion of citrate-capped GNPS in colloidal pseudoboehmite. The suspension was dried at 100 °C followed by annealing in air at temperatures of up to 1000 °C. Thus prepared substrates crystallized in γ-Al$_2$O$_3$ or θ-Al$_2$O$_3$ phases depending on the annealing temperature. XRD, TEM, and Raman spectroscopy characterizations show that GNPS remain nano-crystalline with preserved SERS activity and no apparent changes in size or shape after being treated at high temperatures. These results were also corroborated by the substrate UV-Vis absorption spectra. The SERS enhancement factor for Rhodamine 6G remained stable across the samples and showed no dependence on exposure to harsh environments.

Introduction

The stabilization of noble metals such as gold and silver nano-particles against sintering has attracted recently much attention because of the growing number of applications in the field of catalysis, localized surface plasmon resonance (LSPR), and surface enhanced Raman spectroscopy (SERS).[1–4] The stabilization is achieved by using supporting materials that prevent agglomeration before and during the sintering process. It is well known that the size and shape of the nanoparticles are critical factors to keep them active. However, other factors as size distribution, surrounding environment and surface state also affect the performance of the nanoparticles. The size of the nanoparticles may have a different effect depending on the purpose of application. The best performance of noble metal nanoparticles is usually observed in particles sizing 20 nm or less for catalytic applications[5–7] and in the range of 20–70 nm for SERS.[2]

Several techniques have been developed to deposit metal nanoparticles on different substrates such as TiO$_2$,[8,9] carbon nanostructures[10,11] and more frequently aluminum oxides.[12–15] All those techniques aim to preserve the integrity of the nanoparticles that act as surface enhancer for spectroscopy.[16] Several attempts have been carried out to achieve their stabilization on mesoporous materials. However, these techniques are usually based on complex routes of synthesis or the use of sophisticated equipment, such as PVD, CVD, autoclave, *etc.*, to link or attach the nanoparticles to the substrate.[14,17,18] Additionally, a supporting substrate for stabilization of nanoparticles should meet some general requirements as rough surface, the substrate must have a specific crystallinity and porosity. Materials with such characteristics are capable to immobilize the nanoparticles with an open structure and high surface area for easy access and full interaction with the environment.

Pseudoboehmite (PB) is a hydration phase of finely crystal-line boehmite. PB undergoes several phase transitions with increasing temperature and transforms into γ-Al$_2$O$_3$ (500 °C), θ-Al$_2$O$_3$ (1000 °C), and α-Al$_2$O$_3$ (1200 °C). The γ-Al$_2$O$_3$ phase is most frequently used in applications because of its high porosity, good mechanical properties, thermal stability, and high surface area.[19,20] Here we present a unique synthesis approach that exploits the remarkable affinity of pseudoboehmite to adsorb citrate.[21] The adsorption capacity of functionalized pseudoboehmite has been demonstrated in ref. 21 and 22. As regards to the application side of this property of PB, to the best of our knowledge, there are no reports in the literature describing the use of nanostructured pseudoboehmite powder, particularly for SERS applications, at extreme temperature conditions.

[a] Instituto de Investigaciones Metalúrgicas, Universidad Michoacana de San Nicolás de Hidalgo, Ciudad Universitaria, Michoacán, Mexico

[b] Department of Mechanical Engineering Technology, University of Houston, Houston, TX 77204-4020, USA. E-mail: fcrobles@uh.edu; Tel: +713-743-8231

[c] Instituto of Física and Matemáticas, Universidad Michoacana de San Nicolás de Hidalgo, Ciudad Universitaria, Michoacán, Mexico. E-mail: ptorres80@gmail.com; Tel: +443-322-3500

[d] Centro de Investigaciones en Óptica A.C., Lomas del Campestre, León, Gto., Mexico

[e] Texas Center for Superconductivity and Department of Mechanical Engineering, University of Houston, Houston, TX 77204, USA

[f] Center for Advanced Materials, University of Houston, Houston, TX 77204-4020, USA

This journal is © The Royal Society of Chemistry 2017

J. Mater. Chem. C, 2017, 5, 4959–4966 | 4959

Our strategy for the stabilization of gold nanoparticles (GNPS) in substrate is based on a combination of the properties of as-synthesized pseudoboehmite and gold nanoparticles capped with citrate. GNPS covered with thin layer of sodium citrate (SC) were synthesized following the procedures described in ref. 23 and dispersed in as-synthesized colloidal PB. The derivate and final materials were characterized and documented by means of X-Ray Diffraction (XRD), transmission electronic microscopy (TEM), Ultraviolet-visible spectroscopy (UV-Vis), Fourier transform Infra-red spectroscopy (FTIR) and Raman spectroscopy. The novelty in this work is the attachment of the GPNS to pseudoboehmite colloidal particles through its enhanced adsorption capability to citrate and thus produced substrates sustain exposure to extreme temperatures without deterioration of SERS activity. Additionally, the proposed synthesis can be conducted in a conventional wet lab and requires no sophisticated equipment or complex techniques.

Materials and methods

Materials

Aluminum sulfate hydrate powder ($Al_2O_{12}S_3 \cdot xH_2O$; purity of 98%), gold(III) chloride trihydrate ($HAuCl_4 \cdot 3H_2O$; purity of 99.9%) and sodium citrate ($C_6H_5Na_3O_7 \cdot 2H_2O$; purity 99.0%) were products of Sigma Aldrich. The ammonia anhydrous was delivered from MATHESON. Distilled water and deionized water were used for the synthesis of the pseudoboehmite and gold nanoparticles, respectively.

Synthesis of pseudoboehmite

The pseudoboehmite was synthesized from aluminum sulfate water based solution $(0.2~M)^{24}$ heated at 60 °C in under stirring. During the synthesis commercial ammonia (NH_3) gas was pumped into the solution to reach a pH between 9 and 10:

$$NH_3 + H_2O \rightarrow NH_4^+ + OH^- \tag{1}$$
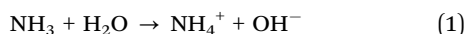
The following reactions show the transitions to pseudoboehmite:

$$Al^{3+} + SO_4^{2-} + NH_4^+ + OH^- \rightarrow AlO(OH) + H_2O + (NH_4)_2SO_4 \tag{2}$$
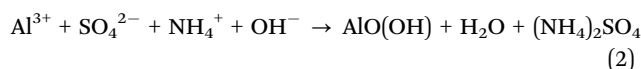
The obtained products were filtered and washed three times with warm distilled water to remove sulfate traces. The end product was pseudoboehmite in form of a white translucent colloid.

Synthesis of gold nanoparticles

The gold nanoparticles were synthesized from gold(III) chloride trihydrate according to the method reported in ref. 23. 50 ml of deionized water and 50 mg of sodium citrate were added into a flask and heated to boiling temperature while stirring. Next, 150 μl of $HAuCl_4$ solution (0.25 M) was added to the boiled mixture and the process was stopped when the solution turned into a ruby-red color.

Sample preparation and SERS substrates

The as-synthesized pseudoboehmite colloid was mixed with 120 ml of colloidal gold nanoparticles in a beaker. The mixture was stirred at room temperature for 60 min followed by a drying process at 100 °C for 24 h. The product was then tested at as-synthesized conditions and after being annealed at temperatures as high as 500 °C and 1000 °C for up to 1 h.

Samples PB/SC1 and PB/SC2 were prepared using 1 g of pseudoboehmite and the respective concentrations of 0.034 M and 0.068 M of sodium citrate. For assessment of SERS performance we used Rhodamine 6G (R6G) as a labeling molecule. A stock solution of R6G in water was prepared at 1×10^{-2} M and further diluted to concentrations of 1×10^{-3}, 1×10^{-4}, 1×10^{-5} and 1×10^{-6} M. Once the dilutions were ready a single droplet (10 μl) of each concentration was mixed with 0.005 g of each SERS substrate in a test tube and dried at room temperature for 24 h. A reference series of substrates was prepared using pseudo-boehmite, γ-Al_2O_3, and θ-Al_2O_3 without gold nanoparticles.

Characterization

A Siemens D5000 diffractometer with a Bragg–Brentano geometry and Cu-Kα radiation (λ = 1.5418 Å) was used to measure X-ray diffraction of the samples at step size = 0.02°, t = 0.5 s, and $10° \leq 2\theta \leq 80°$. Ultraviolet-Visible (UV-Vis) absorption spectra of gold nanoparticles were recorded with a miniature StellarNet spectro-meter EPP2000 in the spectral range from 350 to 800 nm. The reflectance spectra of the thermally treated powders were recorded using a bifurcate optical fiber with the same spectro-meter. The corresponding absorbance spectra were calculated using a sample of pseudoboehmite as reference. The morphology, size, and distribution of gold nanoparticles supported by pseudo-boehmite were analyzed using a transmission electron microscope (TEM, Tecnai F20 Phillips). A TENSOR II Bruker FTIR spectrometer was used for measuring pellets of mixed sample and KBr powders. The Raman characterization was done on a confocal micro-Raman microscope Xplora™, Horiba JY. Laser diodes operating at 532 and 638 nm were used for excitation.

Results and discussion

Fig. 1 shows the XRD patterns of the investigated samples. The presence and stabilization of gold nanoparticles in pseudo-boehmite, γ-Al_2O_3 and θ-Al_2O_3 is evident as well as the phase transitions of pseudoboehmite upon heating to high tempera-tures. The XRD peaks associated with gold were identified in all the samples and correspond to reflections from (111), (200), (220) and (311) planes in good agreement with the reference XRD standard for gold (JCPDS 04-0784). The reflections of the pseudoboehmite correspond to (020), (120), (031), (200), (151), (002) and (251) planes in accordance with the reference standard 21-1307 JCPDS.

The sample exposed to 500 °C shows a complete transformation to γ-Al_2O_3 and lack of pseudoboehmite or other phases in the substrate as confirmed by comparison with 10-0425 JCPDS standard. In the material heated to 1000 °C, the only identified phase is the monoclinic θ-Al_2O_3, 35-0121 JCPDS.

Fig. 2 shows the UV-Vis absorbance spectra for all sample types (as-produced and annealed to high temperatures). The substrates
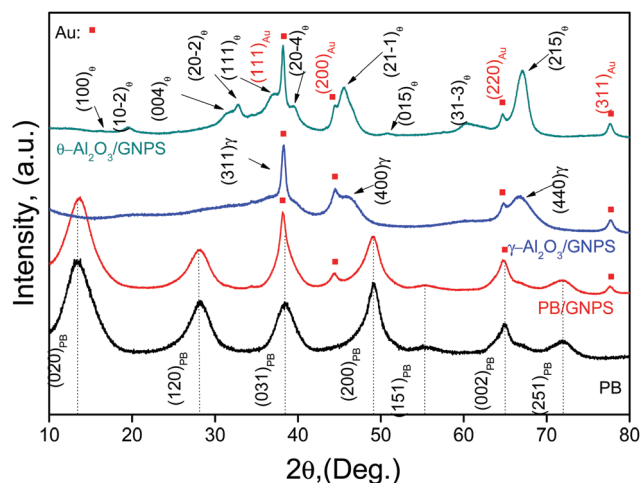
4960 | *J. Mater. Chem. C,* 2017, **5**, 4959–4966

This journal is © The Royal Society of Chemistry 2017

Fig. 1 XRD patterns of pseudoboehmite, PB/GNPS (100 °C), γ-Al$_2$O$_3$/GNPS (500 °C), θ-Al$_2$O$_3$/GNPS (1000 °C). PB, γ, θ, and Au stand for the reflections of pseudoboehmite, γ-Al$_2$O$_3$, θ-Al$_2$O$_3$, and gold, respectively.

with gold nanoparticles were measured by diffuse reflectance using the pseudoboehmite as reference. The gold nanoparticles alone were measured suspended in water. The surface plasmon resonance (SPR) band of gold nanoparticles dispersed in water is located at 530 nm whereas in the case of the powders with GNPS it is red-shifted to 533 nm. The SPR band position and linewidth of GNPS depend on their size, shape, closeness or agglomeration, and on dielectric properties of surrounding media.[16,25] In our case the particle size is preserved during the exposure to high temperatures.

Given the negligible difference between the UV-Vis absorbance spectra of substrates, we conclude that the effective dielectric function (EDF)[26] has minor changes when exposed to high temperatures. The RDF accounts for dielectric function of substrate material components and their geometrical arrangements. In order to explain the SPR band change in going from water dispersed GNPS to SERS substrates one needs to calculate the corresponding EDF using, for instance, the formalism
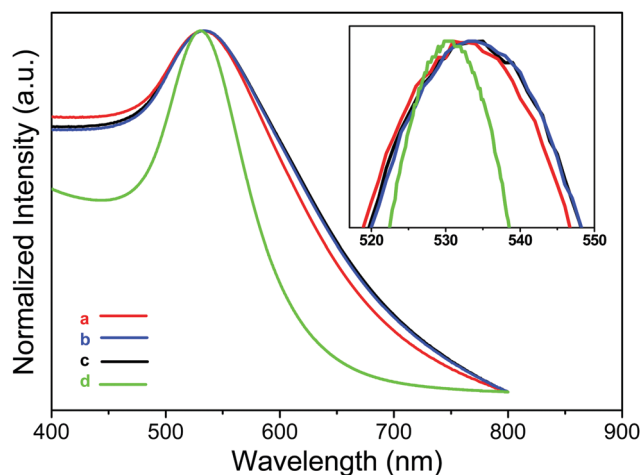

Fig. 2 UV-Vis absorbance spectra of (a) PB/GNPS, (b) γ-Al$_2$O$_3$/GNPS, (c) θ-Al$_2$O$_3$/GNPS as powders, and (d) gold nanoparticles dispersed in water.

described in ref. 26. Such a computational modeling, however, is a study of its alone and beyond the scope of this work.

Fig. 3 shows the TEM characterization of the gold nanoparticles embedded in the pseudoboehmite compared to the sample annealed at 1000 °C. Fig. 3a and b show uniform distribution of the gold nanoparticles in the pseudoboehmite and θ-Al$_2$O$_3$ respectively. Remarkably, in both cases the gold nanoparticles are homogeneously dispersed and the extreme temperature conditions promote no agglomeration. Therefore, our synthesis approach provides a key to preserve the size and distribution of the gold nanoparticles. As a result we produce a SERS active material featuring stable, almost unchangeable, properties with annealing temperature up to 1000 °C.

The size of the gold nanoparticles was determined by measuring at least 100 of them in Digital Micrograph™ software. Thus measured average sizes for the gold nanoparticles are: 21.9 nm ± 2.3 nm, 22.1 nm ± 2.7 nm and 22.7 nm ± 3.3 for the as synthesized, and samples exposed to 500 and 1000 °C respectively. These results support the conclusion that the gold nanoparticles are stable in size, regardless of the temperature treatment.

The substrate annealed at 500 °C recrystallized in the γ-Al$_2$O$_3$ phase exhibiting relatively small grains, high porosity and roughness. The increased surface to volume ratio of γ-Al$_2$O$_3$ grains provides favorable conditions for the gold nanoparticles to seat on the grain surface and being trapped and locked when exposed to even more extreme temperature conditions. The crystallite size of γ-Al$_2$O$_3$ calculated by the Scherrer method was approximately 5 nm.

The FTIR spectroscopy was employed to confirm the adsorption of citrate by pseudoboehmite. The changes in the vibrational bands are caused by the bond configurations of the citrate (monodentate or bidentate) and manifested themselves as band shifts and appearance of specific vibrational bands when the citrate is adsorbed through the carboxylate groups. Fig. 4a compares the FTIR transmittance spectra of pure pseudoboehmite and pure sodium citrate against citrate adsorbed on pseudoboehmite for two concentrations of 0.034 M and 0.068 M denoted by PB/SC1 and PB/SC2, respectively. The spectra of PB/GNPS and pure pseudoboehmite are presented in Fig. 4b and those of PB, θ-Al$_2$O$_3$, and γ-Al$_2$O$_3$ measured over an extended spectral range are shown in Fig. 4c. The FTIR spectra of θ-Al$_2$O$_3$/GNPS and γ-Al$_2$O$_3$/GNPS (not shown here) are essentially the same as those shown in Fig. 4c. The reason is that the citrate caps of GNPS in θ-Al$_2$O$_3$/GNPS and γ-Al$_2$O$_3$/GNPS are burned out and their spectra show no additional bands to those of the substrates without GNPS.

The most prominent vibrational bands of boehmite are at 1640 cm^{-1} and 1064 cm^{-1} that are associated with the stretching and bending vibrations of OH groups in water (ν(OH$_{H_2O}$)) and boehmite (ν(OH$_{AlOOH}$)).[27] In the measured samples we identified those bands at around 1640 cm^{-1} and 1074 cm^{-1}. Additional bands related to H$_2$O were observed at 3400, 3104, 2094, and 1396 cm^{-1} and shown in Fig. 4c. The decrease of H$_2$O vibrational bands intensity after temperature treatments is attributed to dihydroxylation of these materials.

The sodium citrate is characterized by its symmetric (ν_{sym}(COO$^-$)) and asymmetric (ν_{asy}(COO$^-$)) carboxylate vibrational bands
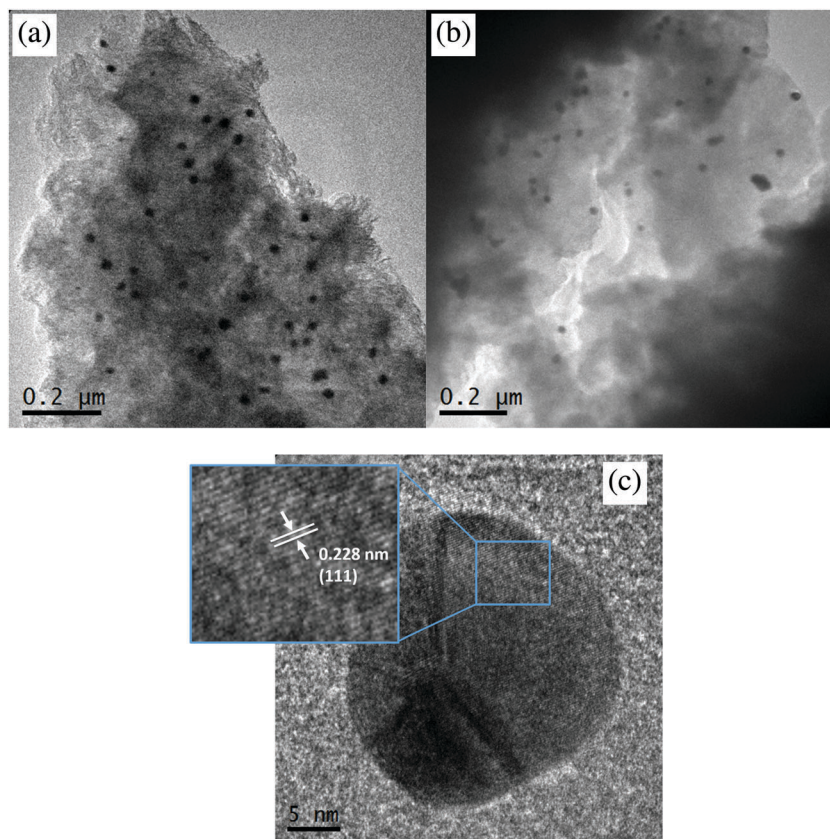
Fig. 3 Images of the Al$_2$O$_3$–gold particles in (a) PB/GNPS (TEM), (b) θ-Al$_2$O$_3$/GNPS (TEM), and (c) HRTEM of a gold particle. The characteristic *d*-spacing of gold is seen for the particle shown in (c).

observed in the spectral ranges 1305–1415 cm^{-1} and 1500–1630 cm^{-1}, respectively.[28] After the adsorption of citrate in pseudoboehmite, some of the sodium citrate bands at 1433 cm^{-1}, 1191 cm^{-1} and 1155 cm^{-1} become undetectable. This indicates that the symmetry of carboxylate was modified and these vibrations lost their infra-red activity. Instead, new bands at 1408 cm^{-1}, 1163 cm^{-1} and 921 cm^{-1} associated with $\nu_{sym}(COO^-)$, $\nu_{sym}(CO)$ and $\nu(CH)$ were detected. This results from the coordination of the carboxylate groups at pseudoboehmite grain surface. The citrate bands of $\nu_{asy}(COO^-)$ at 1660 cm^{-1} and 1593 cm^{-1} shifted to 1625 cm^{-1} and 1585 cm^{-1}, respectively. The other two peaks, assigned to $\nu_{sym}(CO)$, were shifted as well: from 1305 cm^{-1} to 1296 cm^{-1} and from 1276 cm^{-1} to 1267 cm^{-1}.

Fig. 4b compares the FTIR spectra of the samples PB + GNPS and pure pseudoboehmite. The vibrational modes for the PB + GNPS sample correspond to those generated by the coordination of citrate carboxylate groups to both the surface of gold nanoparticles and pseudoboehmite grains. One can also distinguish different vibration modes from those generated when the citrate is coordinated only by pseudoboehmite (Fig. 4a). From Fig. 4a and b we conclude that the variation in vibrational spectra of citrate is due to the different configurations of citrate anchored to pseudoboehmite or gold nanoparticles.

In order to complement the FTIR results, we carried out Raman spectroscopy for the sample PB/SC2. This sample was selected for containing sodium citrate at a higher concentration

and thus producing better resolved Raman spectra. With this characterization we found further evidence of the adsorption of citrate that is associated to the red shift of some of the peaks. Fig. 5 shows the shift of sodium citrate bands associated with $\nu_{sym}(COO^-)$ and $\nu_{asy}(COO^-)$ vibrations as a result of the citrate adsorption. Those bands are usually observed at frequencies of 1440 cm^{-1} and 1598 cm^{-1} and in our case they shifted to a relatively broad band at 1416 cm^{-1} and 1567 cm^{-1}, respectively. Similar frequency shifts were also reported to be due to the adsorption and coordination of the carboxylate groups of citrate on colloidal silver,[29] which was classified in ref. 30 as bidental bonding. Note that the vibrational bands in PB/SC2 at 1416 cm^{-1} and 1567 cm^{-1} are also seen in the FTIR spectra in Fig. 4a.

The intensity of vibrational bands and the extent of frequency shift citrate depend on type of bonding that specifically can be monodentate or bidentate as shown in Fig. 6. The type of bonding. Either monodentate or bidentate, affects the vibration frequencies of the citrate molecule as discussed in ref. 30. Fig. 6 also illustrates the proposed gold particles adsorption mechanism in pseudoboehmite through the monodentate and dominantly bidentate anchoring of the citrate carboxylate groups on pseudoboehmite grains.

The SERS activity of the gold nanoparticles in different substrates was investigated using Rhodamine (R6G) as a labeling molecule. Fig. 7 presents the average SERS spectra of as-synthesized
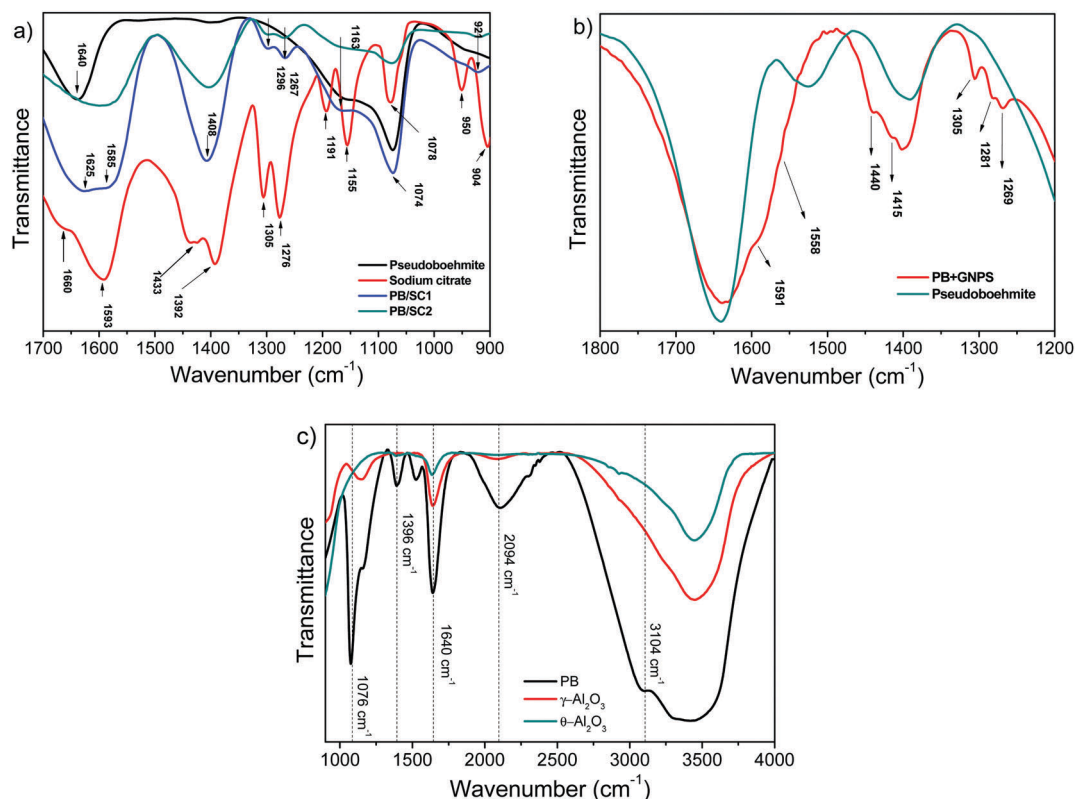
Fig. 4 FTIR characterization of (a) pure pseudoboehmite, pure sodium citrate, PB/SC1 and PB/SC2, and (b) pure pseudoboehmite and PB + GNPS, and (c) PB, θ-Al$_2$O$_3$, and γ-Al$_2$O$_3$ measured over an extended spectral range.
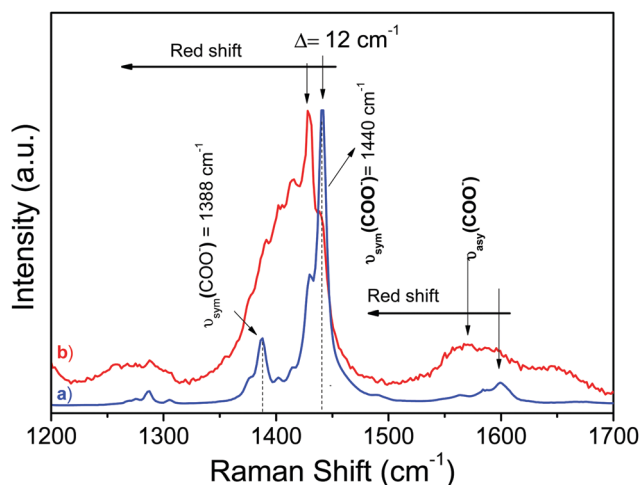

Fig. 5 Raman spectra of pure sodium citrate and PB/SC2. Red shift of the main vibrational bands due to the adsorption of the citrate on pseudoboehmite.

PB/GNPS substrate and those after exposure to temperatures of up to 1000 °C. The Raman confocal mapping of substrates loaded with R6G showed no significant point-to-point variation of the scattering intensity. This result indicates lack of hot spots on the substrates and therefore the matrices (pseudoboehmite, γ-Al$_2$O$_3$ or θ-Al$_2$O$_3$) are homogeneous and form equivalent SERS-sites around the nano-particles. The penetration depth of 638 nm laser light is larger than

the depth of focus of ∼1 μm of the microscope objective 100X used. This simplifies the calculation of SERS enhancement factor (EF) because the two needed measurements that of SERS and no-SERS substrates probe the same scattering volume. The enhancement factor of each substrate was calculated using the equation:[31]

$$\mathrm{EF} = \frac{[I_{\mathrm{SERS}}/N_{\mathrm{surf}}]}{[I_{\mathrm{NRS}}/N_{\mathrm{vol}}]},$$

where I_{SERS} is the surface enhanced R6G Raman intensity, N_{surf} is the number of R6G molecules per unit volume (cm^{-3}) in a layer of thickness equal to the longest dimension of R6G molecule. I_{NRS} is the normal Raman intensity, and N_{vol} is the concentration of R6G molecules in the substrate. Thus calculated EF is of order of 10^3. On the other hand, the minimum detected concentration of R6G on pseudoboehmite substrate without gold nanoparticles was 1×10^{-2} M, whereas for the substrates with gold nanoparticles the minimum detected concentration was 1×10^{-6} M. Therefore, the calculated enhancement factor is 10^3–10^4 for all the SERS substrates. These results give additional confirmation of the successful stabilization of gold nanoparticles.

Unlike the results[32] of using gold nanoparticle colloid annealed at high temperatures as a SERS substrate, we show that the substrates reported in this paper are SERS active in as-synthesized conditions as well as after exposures in extreme environments. This behavior can be attributed to the homogeneous distribution and separation of gold nanoparticles that prevent their coarsening. As a result, the morphology and
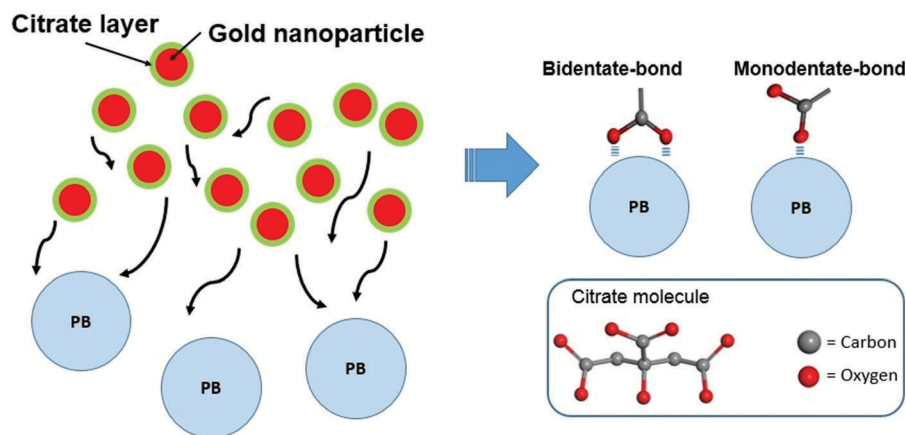
This journal is © The Royal Society of Chemistry 2017

J. Mater. Chem. C, 2017, **5**, 4959–4966 | **4963**

Fig. 6 Adsorption of gold nanoparticles on colloidal pseudoboehmite surface. The two main modes of bonding generated during the adsorption of citrate are shown.
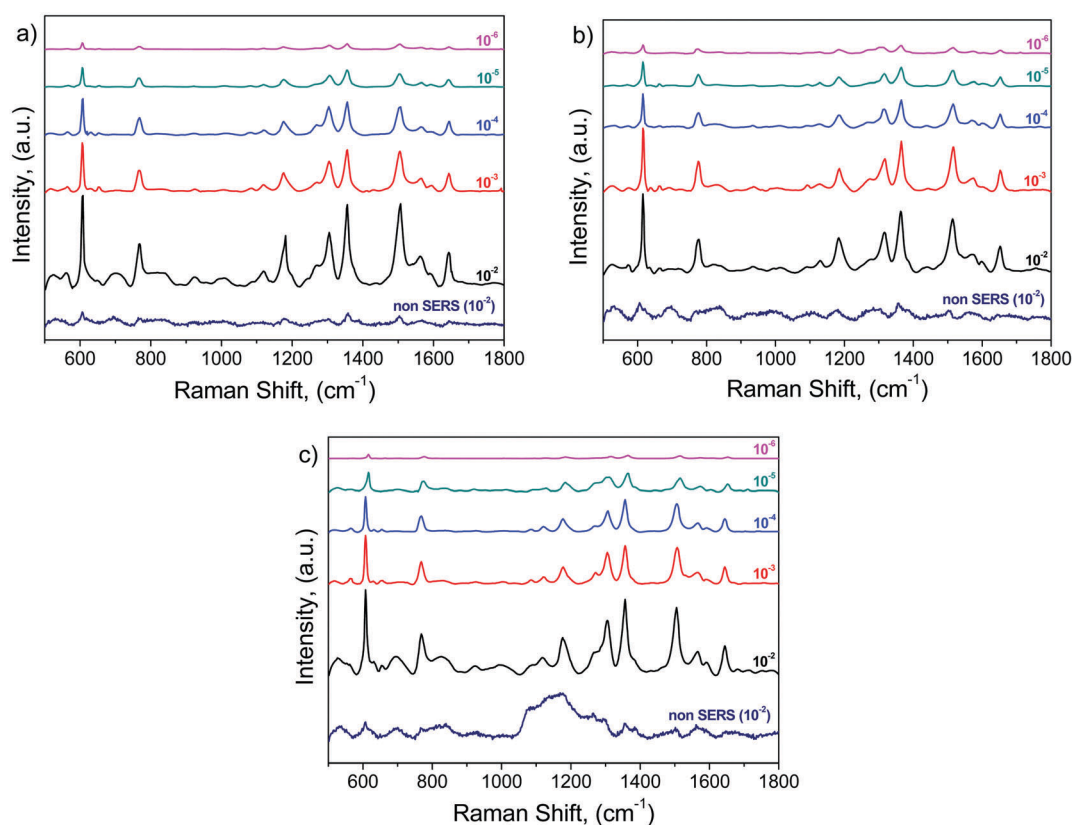

Fig. 7 SERS spectra of R6G solution with different molarity on (a) PB/GNPS, (b) γ-Al$_2$O$_3$/GNPS and (c) θ-Al$_2$O$_3$/GNPS. All measurements were carried out for the same CCD integration time and power density of 638 nm laser excitation.

structural changes of the supporting substrate have no effect on the SERS performance.

In Fig. 8 is presented an example that demonstrates the sustainability of the substrates. One of the possible applications of ultra-high temperatures sustainable SERS substrates is that they can be repeatedly used after purging the substrates by burning the analytes out at high temperatures. Fig. 8b shows the SERS spectra of a substrate initially loaded with 50 µl of R6G solution with a concentration of 10^{-2} M. The 10^{-2} M R6G

spectrum is SERS active and the raw substrate (no R6G) is given for comparison (Fig. 8a). Once the R6G loaded sample is annealed at 1000 °C, the substrate shows no SERS activity or presence of R6G (Fig. 8c). Subsequent loading with the same concentration of R6G shows again a substrate with SERS activity. Furthermore, the intensity is as strong as in the initial SERS measurement (compare Fig. 8b and d). This suggests that the same substrate can be used several times with different analytes. Therefore here we show that once the analyte burns out at
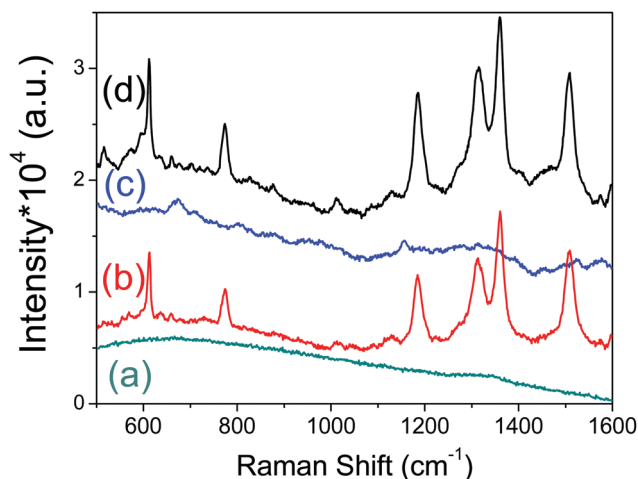
Fig. 8 Raman spectra for the raw sample and SERS active and inactive depending on the heat treatment conditions. (a) Raw sample (θ-Al_2O_3/GNPS), (b) θ-Al_2O_3/GNPS loaded with R6G (SERS active), (c) Al_2O_3/GNPS heat treated at 1000 °C (non SERS active) and (d) θ-Al_2O_3/GNPS heat treated and re-loaded with R6G (SERS active again). All the measurements were carried out at the same integration time.

temperatures as high as 1000 °C the sample can be re-loaded again with the R6G and its SERS activity is preserved. All SERS measurements are carried at room temperature.

Conclusions

We have demonstrated the capability of colloidal pseudoboehmite to adsorb, without clustering, gold nanoparticles capped with sodium citrate. The gold nanoparticles remain homogeneously distributed even when exposed to extreme environments such as annealing at 1000 °C despite the substrate phase transformations from pseudoboehmite to γ-Al_2O_3 or θ-Al_2O_3 and ~30 wt% reduction due to dehydroxylation. Moreover, in this study we show that the SERS substrates can be exposed to temperatures close to the melting temperature of gold without losing their SERS activity. The SERS enhancement is on part with that produced by other substrates with non-clustered gold nanoparticles. Notably, unlike the typical SERS substrates those reported here are bulk substrates, therefore their sensitivity can be improved by increasing the scattering volume probed by Raman spectroscopy rather than the surface area alone accessible in the typical substrates. The substrates can be reused by burning out the analyte followed by an analyte re-loading without losing it SERS activity and sensitivity.

Author contributions

The manuscript was written through contributions of all authors. All authors have given approval to the final version of the manuscript.

Acknowledgements

References

1 N. Lopez and J. K. Nørskov, *J. Am. Chem. Soc.*, 2002, **124**, 11262–11263.
2 H. Ko, S. Singamaneni and V. V. Tsukruk, *Small*, 2008, **4**, 1576–1599.
3 J. Wang, L. Kong, Z. Guo, J. Xu and J. Liu, *J. Mater. Chem.*, 2010, **20**, 5271–5279.
4 T. Noriki, S. Abe, K. Kajikawa and M. Shimojo, *Beilstein J. Nanotechnol.*, 2015, **6**, 1010–1015.
5 D. V. Jawale, E. Gravel, V. Geertsen, H. Li, N. Shah, R. Kumar, J. John, I. N. N. Namboothiri and E. Doris, *Tetrahedron*, 2014, **70**, 6140–6145.
6 C. Lin, K. Tao, D. Hua, Z. Ma and S. Zhou, *Molecules*, 2013, **18**, 12609.
7 S. Sarina, E. R. Waclawik and H. Zhu, *Green Chem.*, 2013, **15**, 1814–1833.
8 V. Iliev, D. Tomova, L. Bilyarska and G. Tyuliev, *J. Mol. Catal. A: Chem.*, 2007, **263**, 32–38.
9 E. Albiter, M. A. Valenzuela, S. Alfaro, G. Valverde-Aguilar and F. M. Martínez-Pallares, *J. Saudi Chem. Soc.*, 2015, **19**, 563–573.
10 R. Zhang, M. Hummelgård and H. Olin, *Mater. Sci. Eng., B*, 2009, **158**, 48–52.
11 H. Ma, L. Wang, L. Chen, C. Dong, W. Yu, T. Huang and Y. Qian, *Catal. Commun.*, 2007, **8**, 452–456.
12 K. Wong-ek, P. Eiamchai, M. Horprathum, V. Patthanasettakul, P. Limnonthakul, P. Chindaudom and N. Nuntawong, *Thin Solid Films*, 2010, **518**, 7128–7132.
13 D. Yin, L. Qin, J. Liu, C. Li and Y. Jin, *J. Mol. Catal. A: Chem.*, 2005, **240**, 40–48.
14 J. Wang, A.-H. Lu, M. Li, W. Zhang, Y.-S. Chen, D.-X. Tian and W.-C. Li, *ACS Nano*, 2013, **7**, 4902–4910.
15 A.-F. An, A.-H. Lu, Q. Sun, J. Wang and W.-C. Li, *Gold Bull.*, 2011, **44**, 217–222.
16 S. Eustis and M. A. El-Sayed, *Chem. Soc. Rev.*, 2006, **35**, 209–217.
17 P. P. Semyannikov, B. L. Moroz, S. V. Trubin, G. I. Zharkova, P. A. Pyryaev, M. Y. Smirnov and V. I. Bukhtiyarov, *J. Struct. Chem.*, 2006, **47**, 458–464.
18 G. M. Veith, A. R. Lupini, S. J. Pennycook, G. W. Ownby and N. J. Dudney, *J. Catal.*, 2005, **231**, 151–158.
19 T. K. Phung, A. Lagazzo, M. Á. Rivero Crespo, V. Sánchez Escribano and G. Busca, *J. Catal.*, 2014, **311**, 102–113.
20 M. Trueba and S. P. Trasatti, *Eur. J. Inorg. Chem.*, 2005, 3393–3403.
21 P. Cambier and G. Sposito, *Clays Clay Miner.*, 1991, **39**, 369–374.
22 A. R. Auxilio, P. C. Andrews, P. C. Junk, L. Spiccia, D. Neumann, W. Raverty, N. Vanderhoek and J. M. Pringle, *J. Mater. Chem.*, 2008, **18**, 2466–2474.

This journal is © The Royal Society of Chemistry 2017

J. Mater. Chem. C, 2017, **5**, 4959–4966 | 4965

23 C. Li, D. Li, G. Wan, J. Xu and W. Hou, *Nanoscale Res. Lett.*, 2011, **6**, 1–10.

24 J. Temuujin, T. Jadambaa, K. J. D. Mackenzie, P. Angerer, F. Porte and F. Riley, *Bull. Mater. Sci.*, 2000, **23**, 301–304.

25 P. Mohan, R. Shinta, J. Fujiwara, H. Takahashi, D. Mott, Y. Matsumura, G. Mizutani, K. Iwami, N. Umeda and S. Maenosono, *Sens. Actuators, B*, 2012, **168**, 429–435.

26 J. Sancho-Parramon, *Nanotechnology*, 2009, **20**, 235706.

27 K. Koichumanova, K. B. Sai Sankar Gupta, L. Lefferts, B. L. Mojet and K. Seshan, *Phys. Chem. Chem. Phys.*, 2015, **17**, 23795–23804.

28 J.-W. Park and J. S. Shumaker-Parry, *J. Am. Chem. Soc.*, 2014, **136**, 1907–1921.

29 H. Tada, J. Bronkema and A. T. Bell, *Catal. Lett.*, 2004, **92**, 93–99.

30 P. Wulandari, T. Nagahiro, N. Fukada, Y. Kimura, M. Niwano and K. Tamada, *J. Colloid Interface Sci.*, 2015, **438**, 244–248.

31 E. C. Le, Ru, E. Blackie, M. Meyer and P. G. Etchegoin, *J. Phys. Chem. C*, 2007, **111**, 13794–13803.

32 K. Zhang, T. Zeng, X. Tan, W. Wu, Y. Tang and H. Zhang, *Appl. Surf. Sci.*, 2015, **347**, 569–573.